



UNIVERSITY OF LEEDS

This is a repository copy of *Observing the emergence of phase biaxiality in a polar smectic A system via polarised Raman spectroscopy*.

White Rose Research Online URL for this paper:

<https://eprints.whiterose.ac.uk/110564/>

Version: Accepted Version

Article:

Zhang, Z orcid.org/0000-0003-2282-3406, Kaur, S orcid.org/0000-0002-8411-8270, Kundu, B et al. (2 more authors) (2017) Observing the emergence of phase biaxiality in a polar smectic A system via polarised Raman spectroscopy. *Journal of Materials Chemistry C*, 5 (5). pp. 1195-1205. ISSN 2050-7526

<https://doi.org/10.1039/C6TC04572C>

© The Royal Society of Chemistry 2017. This is an author produced version of a paper published in *Journal of Materials Chemistry C*. Uploaded in accordance with the publisher's self-archiving policy.

Reuse

Items deposited in White Rose Research Online are protected by copyright, with all rights reserved unless indicated otherwise. They may be downloaded and/or printed for private study, or other acts as permitted by national copyright laws. The publisher or other rights holders may allow further reproduction and re-use of the full text version. This is indicated by the licence information on the White Rose Research Online record for the item.

Takedown

If you consider content in White Rose Research Online to be in breach of UK law, please notify us by emailing eprints@whiterose.ac.uk including the URL of the record and the reason for the withdrawal request.



eprints@whiterose.ac.uk
<https://eprints.whiterose.ac.uk/>

Observing the emergence of phase biaxiality in a polar smectic A system via polarised Raman spectroscopy

Z. Zhang^{a,b}, S. Kaur^{a,c*}, B. Kundu^{a,d}, B. K. Sadashiva^e and H. F. Gleeson^{a,b}

^a*School of Physics and Astronomy, University of Manchester, Manchester, M13 9PL, United Kingdom;* ^b*Present address: School of Physics and Astronomy, University of Leeds, LS2 9JT, United Kingdom;* ^c*Present address: Merck Chemicals, University Parkway, Chilworth, Southampton, SO16 7QD, United Kingdom;* ^d*Present address: Rolic Technologies Ltd, Gewerbestrasse 18, 4123 Allschwil, Switzerland;* ^e*Raman Research Institute, C. V. Raman Avenue, Bangalore 560080, India*

*Corresponding author. Email: h.f.gleeson@leeds.ac.uk

We report polarised Raman spectroscopy, optical and dielectric properties of an asymmetric bent-core compound derived from 3-hydroxybenzoic acid with a long terminal chain at one end and a nitro group at the other. Earlier X-ray scattering experiments on the compound suggested a partial bilayer smectic A phase (SmA_d) and a partial bilayer biaxial antiferroelectric smectic A phase (SmA_dP_A) in the material. The dielectric behaviour, the microscopic textures and conoscopy experiments all explicitly show that the compound exhibits two different phases, with the lower temperature phase biaxial in nature. Raman spectroscopy was used to determine the temperature evolution of the uniaxial order parameters $\langle P_2 \rangle$ and $\langle P_4 \rangle$, deduced from analysis of the depolarisation ratio, informed by modelling the bent-core structure. Anomalously low values were measured (less than 0.5 and 0.15 respectively) which could suggest that the smectic A phase may be de Vries like in nature, rather than a partial bilayer structure. Raman spectroscopy was also used to investigate the biaxial nature of the SmA_dP_A phase. The effect that the biaxial order parameters $\langle P_{220} \rangle$, $\langle P_{420} \rangle$ and $\langle P_{440} \rangle$ has have on the depolarisation ratio is calculated. By making the assumption of an approximately continuous increase in the $\langle P_2 \rangle$ and $\langle P_4 \rangle$ order parameters, it was possible to deduce the behaviour of the biaxial order parameters in the biaxial SmA_dP_A phase; the emergence of biaxial order in the system is clearly demonstrated as all of the biaxial order parameters increase in magnitude as the temperature decreases in the (SmA_dP_A) phase. The dielectric studies show that the perpendicular component of the dielectric permittivity increases from 10 to 70 in the SmA_d phase and decreases from 70 to 45 in the SmA_dP_A phase. A strongly temperature dependent relaxation frequency with a large value

~ 400 kHz is observed in the SmA_d phase. On the other, the SmA_dP_A phase exhibits a weakly temperature dependent relaxation frequency at ~ 100 kHz.

1. Introduction

The last two decades of liquid crystal research have seen an upsurge in the work carried out on liquid crystal molecules with bent-core structures.^{1,2} Researchers' curiosity first arose when Matsunaga and coworkers^{3,4} synthesised achiral bent-core compounds that were seen to form smectic phases exhibiting ferroelectricity, a property previously associated with chiral molecules. A wide variety of interesting discoveries followed, from spontaneous polar order in smectics^{5,6} to the formation of wide variety of phases (denoted B_1 to B_8)⁷ and, more recently, to the formation of the dark conglomerate phase.⁸⁻¹¹ In addition to the tilted phases, the bent-core molecules also form ferroelectric^{12,13} and antiferroelectric¹⁴ orthogonal phases when strong steric interactions are predominant. Indeed the bent-core molecular structure influences the self-organisation within liquid crystal phases, leading to a wide variety of desirable bulk properties, even in the most straightforward phases with orthogonal molecular ordering, the smectic A (SmA) phases. The simplest orthogonal smectic (Sm) phases can be categorised into SmA_1 , SmA_2 or SmA_d phases, depending on the overlap between the molecules in adjacent layers. While the SmA_1 phase exhibits a monolayer structure, SmA_2 displays a bilayer molecular organisation and the SmA_d phase results from the partial interdigitated bilayer structure of molecules.¹⁵

A non-polar but biaxial, orthogonal SmA_d phase was reported by Sadashiva *et al.*^{16, 17} in bent-core compounds, while polar orthogonal phases with antiferroelectric switching ($SmAP_A$) were first reported by Eremin *et al.*¹⁴ In the notation, P refers to polar and the subscript A or F corresponds to antiferroelectric or ferroelectric ordering respectively. Another interesting non-tilted, optically uniaxial, smectic phase is the

$SmAP_R$ where R indicates the random direction of the polarisation in the adjacent layers and which becomes polar in the presence of a field.¹⁸ The $SmAP_R$ phase is reported to exhibit at least one order of magnitude larger relaxation frequency than already reported values in literature, resulting in fast response times desirable for display applications.¹⁹

Biaxiality in smectic A systems has been observed in a number of compounds such as binary mixtures of metallomesogens and 2,4,7-trinitrofluorenone,²⁰ binary mixtures of low molar compounds,²¹ oxadiazoles²² and asymmetric compounds with strong polar groups.^{16, 17} Amaranatha and Sadashiva²³ demonstrated that the biaxial smectic A phase reported earlier^{16, 17} is actually a polar, partially bilayer biaxial smectic A phase, referred to here as SmA_dP_A (note that this notation is sometimes used to explicitly indicate a half-layer interdigitated smectic A phase rather than the partial interdigitation described in Refs 16 and 17). Murthy and Sadashiva²⁴ synthesized a range of asymmetric compounds derived from 3-hydroxybenzoic acid as well as 1,3-dihydroxybenzene. In this paper, we study one of the compounds derived from 3-hydroxybenzoic acid. This compound was shown to exhibit the partial bilayer smectic A phase (SmA_d) and the partial bilayer biaxial antiferroelectric smectic A phase (SmA_dP_A) through x ray studies and preliminary electro-optical switching and textural studies.²⁴

The observation of ferroelectric and antiferroelectric properties in the SmA phases has led to new modes being proposed¹⁸ for electro-optic and scattering displays that were particularly attractive due to their fast response times, bistable switching, and high contrast ratios.^{25,26,27,28} One of the particularly exciting modes is based on a bent-core system exhibiting two SmA_d phases, one with uniaxial and one with biaxial order. The emergence of biaxial order is critical to the display mode and the evolution of the

order at the uniaxial to biaxial phase transition is a subject of significant fundamental interest. This paper offers a new insight into the emergence of the phase biaxiality in polar smectic phases, primarily through polarised Raman spectroscopy (PRS) experiments, supported with other experimental data. We deduce the uniaxial order parameters and demonstrate the emergence of phase biaxiality in the material through a careful analysis of depolarisation ratios deduced from Raman scattering experiments. A key part of the analysis involves modelling of the bent-core molecular structure to inform the analysis of the experimental data and deducing the order parameters *via* fitting the depolarisation ratio. The effect of phase biaxial parameters on the order parameter is considered in detail, revealing the emergence of biaxiality in one of the SmA_d phases. Optical and dielectric observations support the biaxiality deduced from the Raman scattering measurements.

2. Experimental

The bent-core compound studied in this work is an asymmetric compound derived from 3-hydroxybenzoic acid with a long terminal chain at one end and a nitro group at the other end (Fig. 1). The details of the synthesis of this compound are reported in Ref.²⁴. The compound exhibits the following phase sequence observed *via* polarising microscopy while cooling at the rate of (1°C/*min*):

Isotropic 169°C SmA_d 153°C SmA_dP_A 139°C *Crystal*,

There is a narrow biphasic region (2 – 3)°C wide where both the isotropic and the SmA_d phases coexist. The quoted temperatures are the ones when the transition to the low lying phase is complete. The liquid crystalline material was contained in conventional commercial (AWAT, Poland) devices, constructed from parallel glass slides with the inner surfaces treated to promote good, monodomain alignment. 20µm thick homogeneously aligned (SE130 polyimide) devices were used for Raman

spectroscopy measurements, while 5 and 20 μm thick homeotropic aligned (SE-1211 polyimide) devices were used for polarising microscopy and dielectric measurements.

The Raman depolarisation data were collected using a polarised Raman system (Renishaw 1000) comprising of a 515.32 nm, 50 mW solid state laser (Spectra-Physics) and a Leica polarising microscope equipped with a rotatable stage. The temperature controller used was a Linkam TMS93 with a HFS91 hot stage to maintain the temperature with a relative accuracy of ± 0.1 K. The hot stage was mounted on the rotating stage of the microscope. The sample was illuminated by a 50x ultra-long working distance objective lens; ~ 6 mW of laser power was incident at the sample and a 60 second data collection time was used. This combination of the power and collecting time was chosen to obtain a maximum signal to noise ratio, while avoiding any sample heating or degradation. An area with good alignment, much larger than the laser spot ($\sim 2\mu\text{m}$) was selected for the Raman measurements.

The experimental set up for optical and dielectric measurements included a Leica DM 2500P polarising microscope equipped with a Linkam TMS94 temperature controller and LTS350 hot stage, again with a relative temperature accuracy of ± 0.1 K. The polarising microscopy images were recorded using a Delta Pix DP200 camera with a sensor resolution of 1024×768 pixels. The dielectric measurements were carried out using an Agilent Precision LCR Meter E4980A which measures the capacitance and dielectric loss across a frequency range between 20 Hz and 2 MHz using a 0.1 V_{rms} oscillation voltage. The empty devices were calibrated using air as a standard reference to calculate the dielectric permittivity and absorption of the compound under study.

3. Results and discussion

The polarising microscopy, polarised Raman spectroscopy (PRS) and dielectric

measurements were carried out to understand the behaviour of the asymmetric bent-core compound in the SmA_d and SmA_dP_A phases.

Optical measurements

Fig. 2 shows the polarising microscopy textures in a homeotropic (top) and homogeneous (bottom) molecular configuration at various temperatures in the SmA_d ($T - T_{ISmAd} = -7^\circ\text{C}$ and -15°C) and SmA_dP_A ($T - T_{ISmAd} = -17^\circ\text{C}$ and -27°C) phases. An excellent dark homeotropic texture is obtained in the SmA_d phase (Figs. 2a,b). On lowering the temperature to $T - T_{ISmAd} = -16^\circ\text{C}$, i.e., just at the transition between the phases, the dark homeotropic texture changes to a Schlieren texture with domains (Fig. 2c) which become clearer at low temperatures (Fig. 2d). The change in the texture is similar to that observed by Murthy and Sadashiva²⁴ and clearly shows the transition to the SmA_dP_A phase. The homeotropic textures were examined using conoscopy; Fig. 3 shows the Maltese cross observed for the homeotropic uniaxial configuration at ($T - T_{ISmAd} = -7^\circ\text{C}$) (Fig. 3a) which splits indicating a transition to a biaxial phase at the SmA_dP_A transition, $T - T_{ISmAd} = -17^\circ\text{C}$ (Fig. 3b). The distance between the two isogyres increases on further reducing the temperature as can be seen for $T - T_{ISmAd} = -22^\circ\text{C}$ (Fig. 3c), demonstrating both the phase transition from an uniaxial to a biaxial phase and increasing biaxiality with reducing temperature, as was also shown by Murthy and Sadashiva.²⁴

It should be noted that this compound readily adopted a homeotropic alignment geometry, unlike most bent-core materials. However, interestingly, the homeotropic texture starts to transform into a homogeneous texture a few hours after filling the $5\ \mu\text{m}$ device under study. Fig. 4 shows the growing homogeneous texture (bright colour shown in the lower region) at $T - T_{ISmAd} = -13^\circ\text{C}$ with the originally homeotropic

alignment clearly visible as the black texture shown in the upper region of the figure. This transformation suggests a preferred homogeneous alignment of the bent-core molecules pertaining to their molecular structure. Figs. 2e-h show the textural micrographs when the same cell has completely transformed into a homogeneous area. Fine streaks appear on the fan-like structure in the SmA_dP_A phase (Figs. 2g,h), not observed at high temperatures in the SmA_d phase (Figs. 2e,f).

Polarised Raman spectroscopy (PRS) measurements

The PRS technique has been widely used in liquid crystal research²⁹⁻³⁵ to investigate order parameters and to identify phase transitions in rod-like uniaxial systems where both the phases and molecules are uniaxial. In order to describe the orientational order of such systems, we can use the orientational distribution function which consists of a series of Legendre polynomials $P_L(\cos \beta)$ and order parameters $\langle P_L \rangle$ where β is an Euler or polar angle and L is 2, 4, etc. Note that the constraint of L to even values reflects the lack of ferroelectricity in the system and we make the assumption that this is a reasonable approximation in this case even though the lower temperature SmA_dP_A phase is antiferroelectric; the validity of this assumption is discussed in detail later in the paper. The PRS technique allows the determination of both the $\langle P_2 \rangle$ and $\langle P_4 \rangle$ order parameters, an advantage over many other experimental measurements of the order parameter where only $\langle P_2 \rangle$ can be determined. There are a few reports of PRS measurements in bent-core systems³⁴⁻³⁶ and it has been demonstrated that it is especially important to take account of the molecular bend angle in deducing the order parameters in such systems. We deduce both $\langle P_2 \rangle$ and $\langle P_4 \rangle$ in the uniaxial SmA_d phase, taking the molecular bend angle into account. We then apply the same analysis to the SmA_dP_A phase, bearing in mind that the phase is both antiferroelectric and biaxial. While these additional constraints clearly matter, it is not

robust to simply add more fitting parameters to the analysis of the depolarisation ratio. Instead, we examine the influence of biaxiality on the depolarisation ratios deduced in the biaxial SmA_dP_A phase by comparing calculated with the experimental values.

The PRS measurements were carried out in 20 μm thick homeotropic cells with the phases observed on cooling the sample from the isotropic phase. However, the measurements were made when the cell exhibited the homogenous texture due to the interesting configuration transformation mentioned earlier. The quality of the alignment, though good, was not as perfect as for similar measurements on nematic systems. Fig. 5 shows the Raman spectrum obtained for the compound at $T - T_{ISmA_d} = -10^\circ\text{C}$. The corresponding vibrational modes representing the peaks are also mentioned in Fig. 5. The strongest phenyl (C-C) stretching mode at $\sim 1600\text{ cm}^{-1}$ offers the best signal to noise ratio and was used in our PRS analysis. This peak is the one most commonly used in determining order parameters in liquid crystals, satisfying the assumptions associated with the PRS analysis.

To determine the depolarisation ratio, the Raman spectra are measured at intervals of 10° over a complete 360° rotation of the sample around the beam optical axis. The sample rotation is carried out for both parallel and perpendicular polariser-analyser orientations. The C-C stretching peak is fitted with a Lorentzian function to obtain the peak intensity after subtracting the background. The depolarisation ratio for each polarisation angle θ is defined as $R(\theta) = I_{\perp}(\theta)/I_{\parallel}(\theta)$, where $I_{\perp}(\theta)$ and $I_{\parallel}(\theta)$ are the measured intensities for polarisations perpendicular and parallel to the director.

The model used to analyse the Raman data for the bent-core system is fundamentally the same as described in Ref. ³⁶. Fig. 6 shows the bent-core molecule with a bend angle of Ω . The molecular long axis, z_M lies in a certain direction in the molecular bend plane, having the Euler angles (α, β, γ) with respect to the nematic

director \mathbf{n} . The two different Raman active arms (arm 1 and arm 2) are assumed to be along the two mesogenic groups. The arm 1 is tilted from the molecular long axis with an angle β_0 and arm 2 has a bend angle Ω . The molecular angles are used to describe the bent shape of the and appropriately modify the Raman tensor, but the order parameters are determined with respect to the molecular long axis, z_M .

To deduce the order parameters we first obtain the depolarisation ratio for every sample rotation angle θ and then fit the full depolarisation data to Equations 6 and 7 of Ref. ³⁶, allowing us to determine parameters $\langle P_2 \rangle$ and $\langle P_4 \rangle$. Fitting the depolarisation data requires five independent variables: the order parameters $\langle P_2 \rangle$ and $\langle P_4 \rangle$, the differential polarisability ratio r , the bend angle Ω or the tilt angle β_0 and the initial azimuthal angle of the sample with respect to the polarisation plane of the incident beam. In order to reduce the number of fitting parameters, the bend angle Ω for the bent-core compound was set to be 120° (obtained from X-ray results²⁴) so by symmetry $\beta_0 = 30^\circ$.³⁶ It should be noted that for fitting this bent-core system, all the biaxial order parameters including the macroscopic biaxial order parameters (phase biaxiality) and microscopic order parameters (molecular biaxiality) are ignored, leaving only uniaxial order parameters. However we will revisit this approach later in the paper, specifically in the discussion of the data obtained in the low temperature SmA_dP_A phase which is biaxial.

Figs. 7a,b show the order parameters $\langle P_2 \rangle$ and $\langle P_4 \rangle$ as a function of temperature, deduced from fits to the depolarisation ratios. It is seen from Fig. 7a that as the temperature decreases in the SmA_d phase $\langle P_2 \rangle$ and $\langle P_4 \rangle$ increase from 0.46 ± 0.01 to 0.52 ± 0.01 and 0.15 ± 0.01 to 0.18 ± 0.01 respectively. Such values are very low for smectic-A systems. For example measurements in the SmA phase of chiral mixtures are considerably higher, with $\langle P_2 \rangle$ and $\langle P_4 \rangle$ values increasing from 0.55 ± 0.02 to

0.68 ± 0.02 and from 0.25 ± 0.02 to 0.39 ± 0.02 respectively with decreasing temperature.³⁷ In case of 8CB, $\langle P_2 \rangle$ takes values around 0.6 just into the smectic A phase, significantly higher than the value obtained for the asymmetric compound under study here.³⁸ There are very few other reports of $\langle P_2 \rangle$ in the smectic-A phase of bent-core liquid crystals; Pratibha *et al.*³⁹ noted the difficulties of using IR spectroscopy for order parameter measurements, deducing values for S (equivalent to $\langle P_2 \rangle$), that varied significantly (from 0.1 to 0.7) over a 10 K temperature range. The order parameter values seen here are even smaller than those reported in the nematic phase of a series of oxadiazole compounds (varying from $\langle P_2 \rangle \sim 0.4 - 0.8$ and $\langle P_4 \rangle \sim 0.25 - 0.5$).³⁵ This interesting result suggests that the bent structure inhibits the nematic-like orientational order of the molecules within the smectic layers, resulting in a low value of $\langle P_2 \rangle$ reminiscent of the behaviour in the de Vries phase.⁴⁰ Indeed the smectic layer spacing of homologues of the material under study here is reported to be considerably smaller than the molecular length (Ref. ²⁴), which leads to the suggestion that the structure is interdigitated SmA_d . We note that we can rule out the possibility that the low order parameters are a consequence of not taking into account the fact that the Raman signal comes from two arms of the molecule with a bend angle between; taking the molecular bend properly into account is a feature of our work as described in Refs. 36 and 41. Also, although our alignment in the smectic phase is less perfect than in a nematic phase, it is still good and so cannot account for such low order parameters (the alignment is comparable to that in Ref [37] where much higher order parameters are reported in the SmA phase). Our order parameter results suggest that an alternative explanation for such behaviour is low nematic order within the layers and a possible de Vries-like structure in the smectic-A phase, though further experiments and/or an

analysis of our data with a different ODF in the model would be necessary to validate this suggestion.

We now consider the order parameter data deduced from the depolarisation ratio measurements in the biaxial SmA_dP_A phase deduced using the same assumptions and approach as for the SmA_d phase. Figs. 7a,b show that $\langle P_2 \rangle$ and $\langle P_4 \rangle$ evaluated in this way decrease with reducing temperature from 0.52 ± 0.01 and 0.18 ± 0.01 to 0.50 ± 0.01 and 0.14 ± 0.01 respectively. The temperature at which we observe a decrease in $\langle P_2 \rangle$ and $\langle P_4 \rangle$ coincides with the SmA_d to the SmA_dP_A phase transition temperature determined *via* polarising microscopy and conoscopy, showing that the Raman data accurately reflect that a phase transition has occurred. However, the fact that the order parameters decrease rather than increasing with reducing temperature is unexpected and we consider several possible explanations.

A useful approach to understanding the Raman scattering data in the SmA_dP_A phase is to examine the depolarisation ratio data directly. The simplest possible analysis is to associate an increase in the magnitude of the depolarisation ratio with an increase in the order parameter of the material. Fig. 8 shows the depolarisation ratio plots in the SmA_d (at $T - T_{ISmA_d} = -5$ °C and -15 °C) and the SmA_dP_A phase (at $T - T_{ISmA_d} = -21$ °C), together with fits to the data. As is expected, the magnitude of the depolarisation ratio increases as the temperature in the SmA_d phase decreases reflecting the increase in the order parameter deduced from the fitting. However, the magnitude of the depolarisation ratio decreases only very slightly in the SmA_dP_A phase, suggesting that any decrease in order parameters would be smaller than the values the graph imply. Further, the shape of the depolarisation ratio has changed significantly in the SmA_dP_A , a factor that we consider later. It is important to emphasise that despite the apparent change in shape of the fitting curves in Fig. 8, all three have been fit using the

same (uniaxial) model. The slightly noisy depolarization ratio data at 90° and 270° are primarily a consequence of the very small perpendicular signal obtained for this material, observed in both the planar and homeotropic samples, not poor sample alignment. As we have shown previously³⁵, the fit at these positions is relatively insensitive to $\langle P_2 \rangle$, with a bigger influence on $\langle P_4 \rangle$, so would not affect our conclusions regarding the anomalously small value of $\langle P_2 \rangle$. The emergence of a different shape in the SmA_dP_A phase is considered further below.

The next assumption that must be tested is that of a constant bend angle of 120° across both smectic phases; it is certainly possible that the bend angle changes with temperature. The sensitivity of our analysis to changes in the bend angle was examined by comparing the two calculated depolarisation curves in Fig. 9. The black curve represents a fit to the data at $T - T_{ISmA_d} = -21^\circ\text{C}$, with fitting parameters: $\langle P_2 \rangle = 0.496$; $\langle P_4 \rangle = 0.153$; $r = -0.294$ and $\Omega = 120^\circ$. The red curve is calculated using different fitting parameters; we assumed that the order parameters had changed as indicated by the extrapolation in Fig. 7, with $\langle P_2 \rangle = 0.535$ and $\langle P_4 \rangle = 0.188$ and looked for the best fit to the data allowing both r and Ω to vary. The red curve in Fig. 9 is the result and the relevant parameters are $r = -0.284$ and $\Omega = 118^\circ$. The bend angle has changed by only 2° in each process, indicating that it is not an important parameter in the fitting. Indeed, the red curve in Fig. 9 represents a worse fit to the data, notable in the lowest part of the curve at angles $\sim 180^\circ$ where the red curve is too low to fit the data. In contrast, all of our other analyses fit this part of the data set extremely well. The conclusion is in line with other examples of such analyses which demonstrated that the order parameters depend relatively weakly on the molecular bend, requiring significant changes (of the order of tens of degrees) to result in large changes in order parameter.^{36,41}

We now consider more complex explanations for the anomalous data in the SmA_dP_A phase. Earlier, we mentioned that the fitting in the SmA_dP_A phase was based on the assumption of a uniaxial, non-ferroelectric system. The apparent decrease in both $\langle P_2 \rangle$ and $\langle P_4 \rangle$ in the SmA_dP_A phase could well be a consequence of neglecting the ferroelectric and biaxial properties of the system in our model; indeed the conoscopy results (Fig. 3) clearly demonstrate the phase biaxiality of the biaxial SmA_dP_A phase. However, as already noted, adding more parameters can cause degeneracy in the fitting so we consider the influence of the phase biaxial order parameters as follows.

In order to discuss biaxiality, we now introduce notation of the form $\langle P_{Lmn} \rangle$ to represent the order parameters as described in earlier papers.³⁴⁻³⁶ In this notation, L is as defined earlier, while m and n correspond to phase biaxiality and molecular biaxiality respectively. The value of m and n is always an even number and smaller or equal to L due to symmetry assumption. In addition, when there is no phase or molecular biaxiality, m and n are zero. Thus, $\langle P_2 \rangle$ and $\langle P_4 \rangle$ can be expressed as $\langle P_{200} \rangle$ and $\langle P_{400} \rangle$ respectively and the phase biaxial order parameters can be denoted by $\langle P_{220} \rangle$, $\langle P_{420} \rangle$ and $\langle P_{440} \rangle$. We are still neglecting molecular biaxiality, in common with all other treatments of Raman scattering from liquid crystals. As a consequence, we can express the depolarisation ratio in terms of five order parameters, i.e., $\langle P_{200} \rangle$, $\langle P_{400} \rangle$, $\langle P_{220} \rangle$, $\langle P_{420} \rangle$ and $\langle P_{440} \rangle$. It is noteworthy that the biaxial order parameters which are deduced describe biaxial order of long molecular axes and not the degree or ordering of transverse dipoles; indeed consideration of the dipolar order would require further modification to the theory. The equations for the Raman intensity when the analyzer is parallel (I_{\parallel}) and perpendicular (I_{\perp}) to the polarizer are:

$$I_{\parallel} = \frac{2}{15} (5(1 + 2r + 3r^2) + (-1 + r)^2 \cos 2\Omega)$$

$$\begin{aligned}
 & -\frac{1}{42}\langle P_{200} \rangle (-1+r)(5+9r - (-1+r)\cos 2\Omega + 3(3+4r)\cos 2\chi \\
 & \quad + 3(3+4r)\cos 2(\chi + \Omega))(1+3\cos 2\theta) \\
 & + \frac{1}{17920}\langle P_{400} \rangle (-1+r)^2(6\cos 2\Omega + 5(6+8\cos 2\chi + 7\cos 4\chi + 8\cos 2(\chi + \Omega)) \\
 & \quad + 7\cos 4(\chi + \Omega) + 14\cos 2(2\chi + \Omega))(9+20\cos 2\theta + 35\cos 4\theta) \\
 & - \frac{2}{7}\langle P_{220} \rangle (-1+r)(5+9r - (-1+r)\cos 2\Omega + 3(3+4r)\cos 2\chi \\
 & \quad + 3(3+4r)\cos 2(\chi + \Omega))\sin^2 \theta \\
 & + \frac{3}{224}\langle P_{420} \rangle (-1+r)^2(6\cos 2\Omega + 5(6+8\cos 2\chi + 7\cos 4\chi + 8\cos 2(\chi + \Omega)) \\
 & \quad + 7\cos 4(\chi + \Omega) + 14\cos 2(2\chi + \Omega))(5+7\cos 2\theta)\sin^2 \theta \\
 & + \frac{1}{32}\langle P_{440} \rangle (-1+r)^2(6\cos 2\Omega + 5(6+8\cos 2\chi + 7\cos 4\chi + 8\cos 2(\chi + \Omega)) \\
 & \quad + 7\cos 4(\chi + \Omega) + 14\cos 2(2\chi + \Omega))\sin^4 \theta \\
 I_{\perp} = & \frac{1}{30}(-1+r)^2(5+3\cos 2\Omega) \\
 & + \frac{1}{84}\langle P_{200} \rangle (-1+r)^2(1+3\cos 2\Omega + 6\cos 2\chi + 6\cos 2(\chi + \Omega)) \\
 & - \frac{1}{17920}\langle P_{400} \rangle (-1+r)^2(6\cos 2\Omega + 5(6+8\cos 2\chi + 7\cos 4\chi + 8\cos 2(\chi + \Omega)) \\
 & \quad + 7\cos 4(\chi + \Omega) + 14\cos 2(2\chi + \Omega))(-3+35\cos 4\theta)) \\
 & + \frac{1}{14}\langle P_{220} \rangle (-1+r)^2(1+3\cos 2\Omega + 6\cos 2\chi + 6\cos 2(\chi + \Omega)) \\
 & + \frac{3}{896}\langle P_{420} \rangle (-1+r)^2(6\cos 2\Omega + 5(6+8\cos 2\chi + 7\cos 4\chi + 8\cos 2(\chi + \Omega)) \\
 & \quad + 7\cos 4(\chi + \Omega) + 14\cos 2(2\chi + \Omega))(1+7\cos 4\theta)) \\
 & + \frac{1}{128}\langle P_{440} \rangle (-1+r)^2(6\cos 2\Omega + 5(6+8\cos 2\chi + 7\cos 4\chi + 8\cos 2(\chi + \Omega)) \\
 & \quad + 7\cos 4(\chi + \Omega) + 14\cos 2(2\chi + \Omega))\sin^2 2\theta
 \end{aligned}$$

The influence of the phase biaxial order parameters $\langle P_{220} \rangle$, $\langle P_{420} \rangle$ and $\langle P_{440} \rangle$ on the depolarisation ratio plots for the biaxial SmA_dP_A phase is best illustrated *via*

calculation. Figs. 10a-c show the effect of varying the phase biaxial order parameters $\langle P_{220} \rangle$, $\langle P_{420} \rangle$ and $\langle P_{440} \rangle$ respectively on the depolarisation ratio in the biaxial SmA_dP_A phase. In each of these plots, one phase biaxial order parameter is allowed to change while others are not (this is a similar approach to that first reported in Ref. ³⁵ and is designed to give an insight into the relative influence of the different phase biaxial order parameters. Fig. 10a shows the calculated depolarisation ratios when $\langle P_{220} \rangle$ is allowed to take two values (0 (black line) and 0.05 (red line)) while $\langle P_{420} \rangle$ and $\langle P_{440} \rangle$ are fixed at zero. With $\langle P_{220} \rangle = 0.05$, the depolarisation ratio curve (red curve) is dramatically changed from that determined experimentally (the black curve), with a significant decrease in R at 90° and 270° and a slight increase at 0° and 180° . Fig. 10b illustrates the effect of an increase in the value of $\langle P_{440} \rangle$ from 0 (black line) to 0.005 (red line) while keeping the other biaxial parameters at zero. Again, we see a reduction in R at 90° and 270° , though the effect is not so marked as for $\langle P_{220} \rangle$. However, there is no obvious change in R at 0° and 180° in this case. Finally, we consider the effect of changing $\langle P_{420} \rangle$, Fig. 10c. The effect on R is very different from that caused by changing $\langle P_{220} \rangle$ and $\langle P_{440} \rangle$. Changing $\langle P_{420} \rangle$ from 0 to 0.005 causes R to increase at 90° and 270° (unlike in cases of $\langle P_{220} \rangle$) and also at 0° and 180° , similar to the change caused by an increase in $\langle P_{220} \rangle$. Clearly, including the biaxial order parameters $\langle P_{220} \rangle$, $\langle P_{440} \rangle$ and $\langle P_{420} \rangle$ has a significant influence on form of the depolarisation ratio.

Given the clear indication that the biaxial order parameters should be included in our analysis, we devised an approach that would potentially give insight into their evolution whilst avoiding the possible degeneracy associated with simply fitting the experimental data with a large number of variables. We achieved this by fixing $\langle P_{200} \rangle$ and $\langle P_{400} \rangle$ to the values in the extrapolated curves in Figs. 7 a and b and maintaining the molecular bend angle at 120° , an approach that leaves only 4 independent fitting

parameters. Fig. 11 shows the results of such an analysis; all of the phase biaxial order parameters increase as a function of decreasing temperature in the biaxial SmA_dP_A phase. It is fair to assume that the relative magnitudes and the temperature dependence of these parameters are reasonable, though the absolute values cannot be relied on (they depend on our assumptions about $\langle P_{200} \rangle$ and $\langle P_{400} \rangle$). As can be seen from Fig. 12, the fitting curve that includes the biaxial order parameters is in excellent agreement with the experimental data. This careful approach, avoiding degeneracy in the fitting process, demonstrates the growing biaxial order in the biaxial phase, proving that PRS is a useful tool for understanding order in complex liquid crystal phases.

Dielectric measurements

Capacitance measurements were also carried out to determine both the perpendicular and the parallel components of dielectric permittivity in homogenous and homeotropic configurations respectively, throughout the SmA_d and SmA_dP_A phases. As mentioned earlier, the $5 \mu m$ thick homeotropic aligned cell was first used to determine the parallel component of dielectric permittivity. The alignment in the cell later changed to homogeneous configuration, therefore the perpendicular component of dielectric permittivity was also determined in the same cell.

In case of homogeneous alignment of the material, the real part of dielectric permittivity, ϵ'_{\perp} increases in the SmA_d phase, reaching a maximum and then decreases in the SmA_dP_A phase as seen in Fig. 13a. The increase in ϵ'_{\perp} from 10 to 70 with the decreasing temperature in the SmA_d phase is expected due to the increasing dipole-dipole interaction with reducing temperature, the usual behaviour for a smectic A phase. The increase in permittivity is large in comparison with standard rod-like compounds (8CB exhibits a value of ~ 10 in the SmA phase), but is in line with what would be expected for such a large bent-core compound. In the SmA_dP_A phase, the dielectric

permittivity is an average of two components and decreases with the decreasing temperature due to antiferroelectric ordering, behaviour also exhibited by standard antiferroelectric compounds.⁴² Fig. 13b explicitly shows the dielectric permittivity ϵ'_{\perp} as a function of frequency at a few temperatures in the SmA_d phase. The dielectric permittivity attains a maximum value of ~ 70 in the SmA_d phase and then starts to decrease in the SmA_dP_A phase (as shown in the inset). The dipolar contributions to the high dielectric permittivity cease at around a few hundred kHz, where large absorption peaks are observed (Fig. 13c). Fig. 13c explicitly shows the imaginary part of dielectric permittivity (ϵ''_{\perp}) as a function of frequency at various temperatures in the SmA_d phase. A strongly temperature dependent dielectric absorption peak is observed throughout the SmA_d phase. The relaxation frequency (the frequency at which the dielectric absorption is maximum) decreases to a lower frequency as the temperature decreases from $T - T_{ISmA_d} = -4^{\circ}\text{C}$ ($\nu_R = 441 \text{ kHz}$) to $T - T_{ISmA_d} = -15^{\circ}\text{C}$ ($\nu_R = 77 \text{ kHz}$)(Fig. 13c). The relaxation frequency found for the SmA_d phase is very high and can be compared to a similarly high value reported by Gupta *et al.*¹⁹ in the SmA_dP_R phase. Clearly, the SmA_d phase of the compound in this work is different from the SmA_dP_R phase reported by Gupta *et al.*¹⁹ One key difference is in the polarisation reversal current which is large in case of SmA_dP_R ¹⁹ whereas no polarisation peak is found in case of SmA_d phase.²⁴

The dielectric absorption peak is weakly temperature dependent (increases with decreasing temperature) in the lower temperature SmA_dP_A phase (inset to Fig. 13c). However, the dielectric absorption value is high (~ 30) in comparison with the conventional SmA phase.⁴³ Kruger and Giesselmann⁴³ also observed high values of ~ 20 -30 in a de Vries SmA phase. Such high dielectric absorption values thus lend support to our suggestion of a de Vries-like structure in the smectic-A phase of the

studied compound. Finally, we note that Guo *et al.*⁴⁴ also reports high dielectric permittivity and relaxation frequency in the SmA_dP_A phase for a similar bent-core structure and terminal chain length but instead of a nitro group exhibits a cyano group.

In the homeotropic configuration, the dielectric permittivity ϵ'_{\parallel} in the SmA_d and SmA_dP_A phase was found to be much lower ≈ 3 (Fig. 13d) than the perpendicular component where it varied from 10 to 70 (Fig. 13b). However, the dielectric permittivity in the homeotropic configuration (Fig. 13d) increases in the SmA_d phase and decreases in the SmA_dP_A phase on decreasing the temperature. A similar increase in the dielectric permittivity was observed in the SmA_d phase followed by a decrease in the SmA_dP_A phase in case of homogeneous configuration (Fig. 13a). No reports are published to our knowledge on the homeotropic configuration in the orthogonal smectic phases.

Conclusions

In summary, we have investigated an asymmetric bent-core compound exhibiting phases identified as SmA_d and SmA_dP_A phases using microscopy, conoscopy, PRS and dielectric measurements. The bent-core compound could be aligned homeotropically, which interestingly transformed into a homogeneous texture in the same cell after a few hours. The textures in both homogeneous and homeotropic geometry allowed a clear distinction between the SmA_d and SmA_dP_A phases. Conoscopy further confirmed the biaxial nature of the phase had been previously inferred *via* X-ray scattering.²⁴

Polarising Raman spectroscopy has successfully been applied to both the smectic phases and order parameters $\langle P_2 \rangle$ and $\langle P_4 \rangle$ deduced. Several interesting conclusions can be drawn. Firstly, the order parameters in the higher temperature smectic A phase were found to be anomalously low, suggesting that it has similarities to a smectic A de Vries structure. This observation is also of relevance to recent theoretical

work by Osipov and Pajak who made the assumption of perfect ordering in their molecular theory of antiferroelectric and ferroelectric ordering in bent-core molecules; at least in this system, such an assumption is not appropriate. Applying the uniaxial fitting method to PRS data in both phases clearly reveals the phase transition between the phases. We were also able to show that there was no evidence of a strong variation in the molecular bend angle as a function of temperature. A careful analysis of the depolarisation ratio curves allowed insight into the relative influence of the biaxial order parameters. By making the assumption that the $\langle P_2 \rangle$ and $\langle P_4 \rangle$ order parameters increase approximately continuously across the uniaxial to biaxial phase transition, it was possible to deduce biaxial order parameters in the SmA_dP_A phase. Although our approach does not allow the actual magnitude of the biaxial order parameters to be determined, we showed that they all increased with decreasing temperature, as expected, and that $\langle P_{220} \rangle$ was the most important biaxial order parameter for this system.

Both the perpendicular and parallel components of the dielectric permittivity increased with decreasing temperature in the SmA_d phase and decreased in the SmA_dP_A . Such behaviour is analogous to that found for a standard SmA phase and an antiferroelectric phase. However, the dielectric permittivity exhibited larger values in both the phases than is normally observed for rod like compounds. The perpendicular component of the dielectric permittivity was found to be much higher than the parallel component due to the strong longitudinal nitro group. A strongly temperature dependent relaxation frequency starting $\sim 400 \text{ kHz}$ was obtained in the SmA_d phase, similar to a relaxation reported in the SmA_dP_R phase in a similar bent-core compound. This large relaxation frequency will result in relatively fast electro-optic response times, making this compound an excellent contender for display applications. In the SmA_dP_A phase,

the relaxation frequency is weakly temperature dependent and found to be ~ 100 kHz. Both the anomalously low order parameter results and the high dielectric absorption observed in the SmA_dP_A phase, suggest that the phase under study could potentially be a de-Vries like phase. However, further experimental evidence is required to prove such a suggestion.

Acknowledgements and notes

This work was supported by the Engineering and Physical Sciences Research Council under Project no. EP/G023093/1. ZZ and SK would like to acknowledge the Universities of Manchester and Leeds for financial support. The original data for the experiments reported in this paper can be found at <http://doi.org/10.5518/117>.

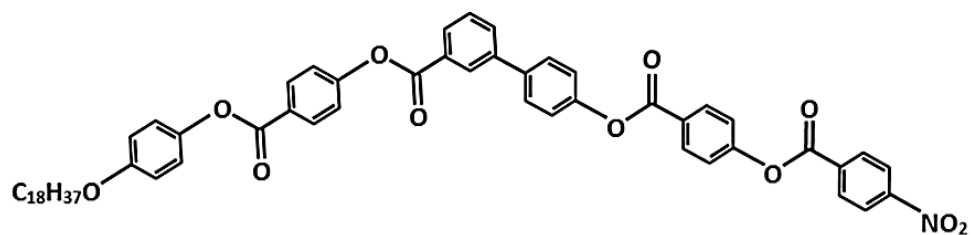


Fig. 1 The molecular structure of the asymmetric compound used in this work.

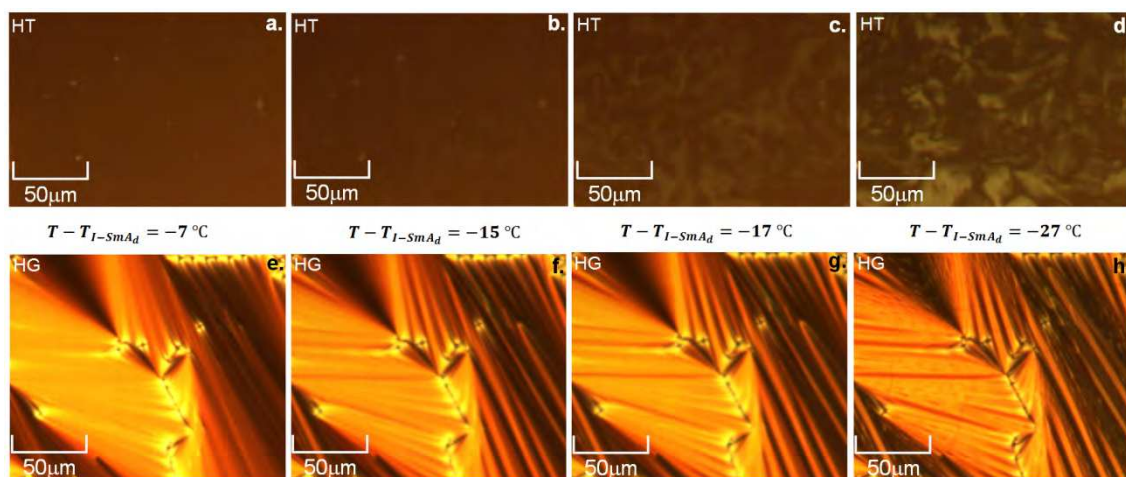


Fig. 2 Polarising microscopy textures of the compound during cooling at different temperatures with the SmA_d phase shown in (a,b) and (e,f) and SmA_dP_A phase shown in (c,d) and (g,h). The textures on the top (a-d) and below (e-h) are taken respectively in a homeotropic and a homogenous orientation of the compound in the same cell.

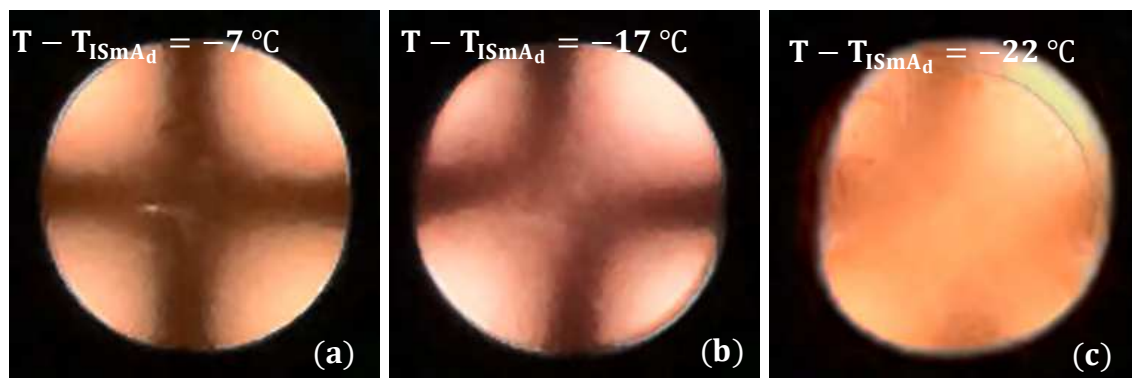


Fig. 3 Conoscopic images in (a) the SmA_d phase and (b,c) in the SmA_dP_A phase. The cross representing (a) the uniaxial phase at $T - T_{ISmA_d} = -7\text{ }^\circ\text{C}$ splits into two isogyres at $T - T_{ISmA_d} = -17\text{ }^\circ\text{C}$ and $-22\text{ }^\circ\text{C}$ in (b) and (c) respectively showing an evidence for the biaxial nature of the phase at these temperatures.



Fig. 4 The growth of the homogeneous texture in a 5 μm homeotropic aligned cell in the SmA_d phase at $T - T_{ISmAd} = -13^\circ\text{C}$.

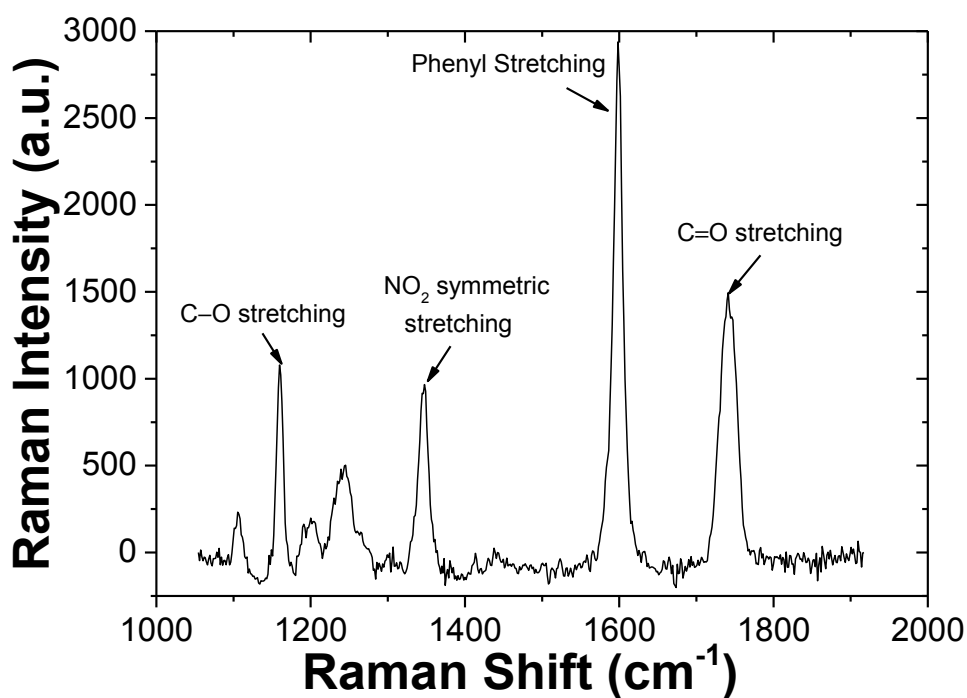


Fig. 5 The Raman spectrum of the compound under study at $T - T_{\text{ISmAd}} = -10\text{ }^{\circ}\text{C}$ showing peaks for C-O stretching (1167 cm^{-1}), NO₂ symmetric stretching ($1360 - 1320\text{ cm}^{-1}$), phenyl stretching (1606 cm^{-1}) and C=O stretching (1750 cm^{-1}). The strongest phenyl stretching mode at $\approx 1600\text{ cm}^{-1}$ was used to determine the order parameters.

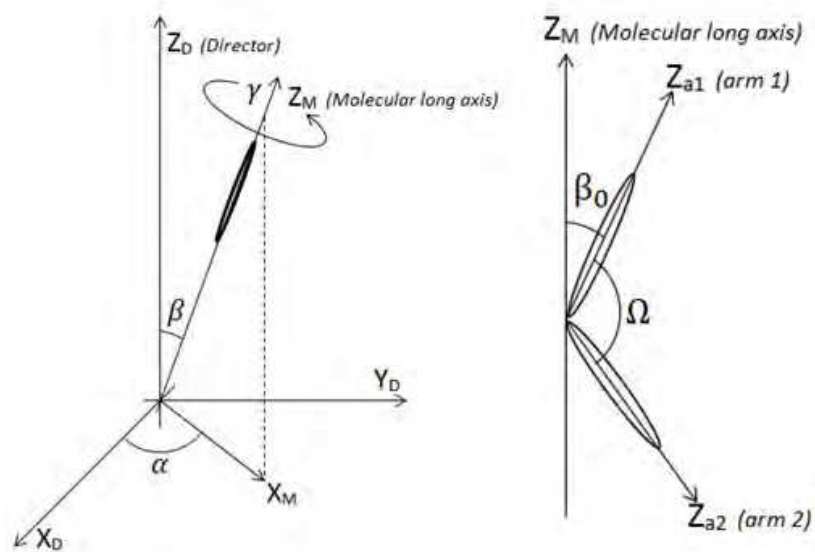


Fig. 6 An illustration of the fitting model used. We assume the bent molecule has one arm (arm 1) tilted from the molecular long axis with an angle β_0 and the other arm (arm 2) has a bend angle Ω . The molecular long axis behaves as a normal rod-like molecule.

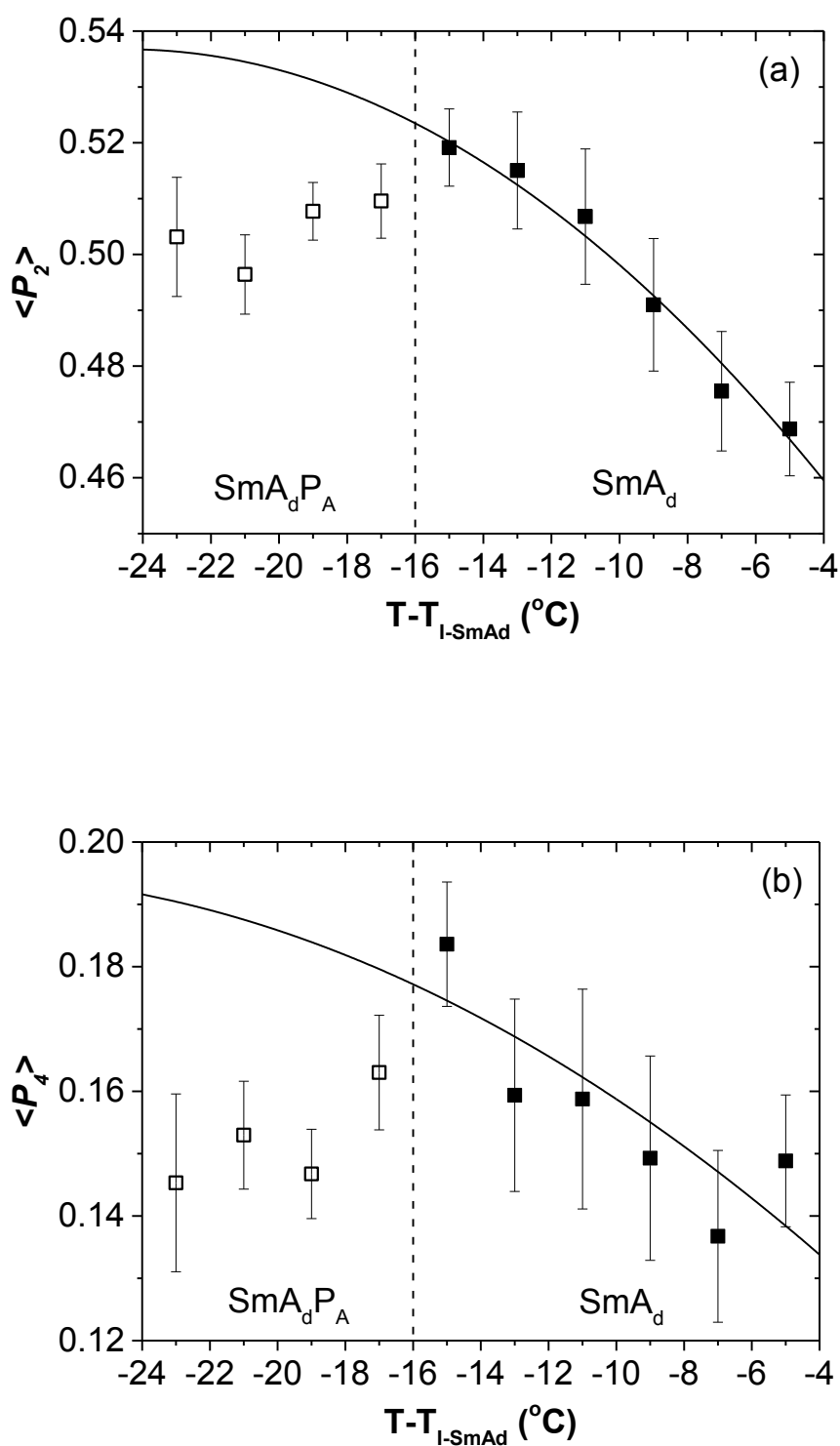


Fig. 7 The uniaxial order parameters deduced from fits to the Raman depolarisation ratio (a) $\langle P_2 \rangle$ and (b) $\langle P_4 \rangle$ at different temperatures in the SmA_d and SmA_dP_A phase. The lines drawn are a guide to the eye in order to show an increasing order parameter in the low temperature, higher order phase.

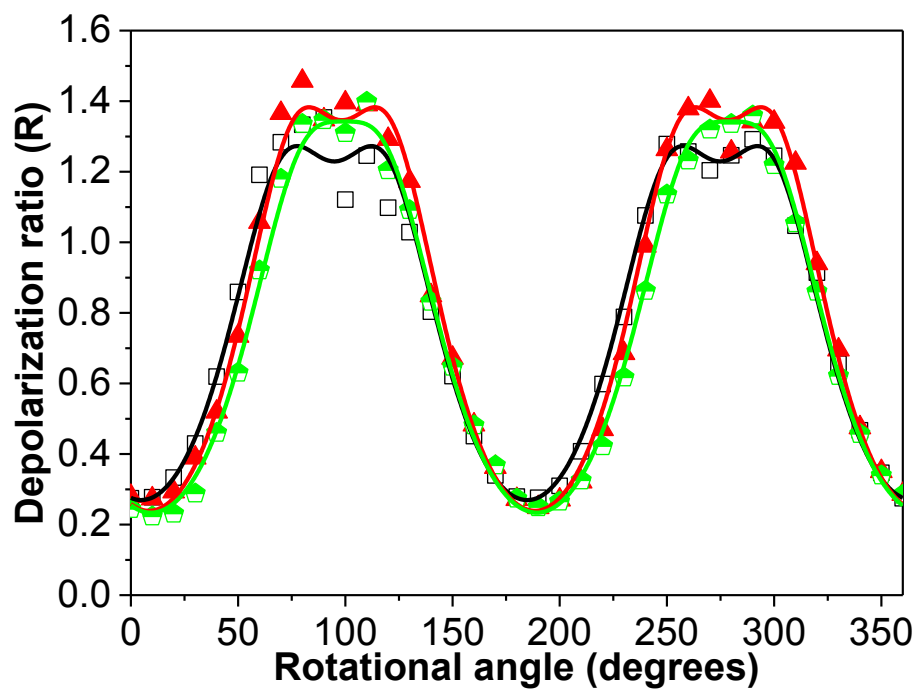


Fig. 8 (Online colour) The depolarisation ratio, R plotted as a function of rotational angle around the optical axis of the laser beam at $T - T_{ISmA_d} = -5^\circ\text{C}$ (open black square) and -15°C (closed red square) in the SmA_d phase and at $T - T_{ISmA_d} = -21^\circ\text{C}$ (half closed green pentagon) in the SmA_dP_A phase. The corresponding coloured lines show the fitting performed using the uniaxial fitting model.

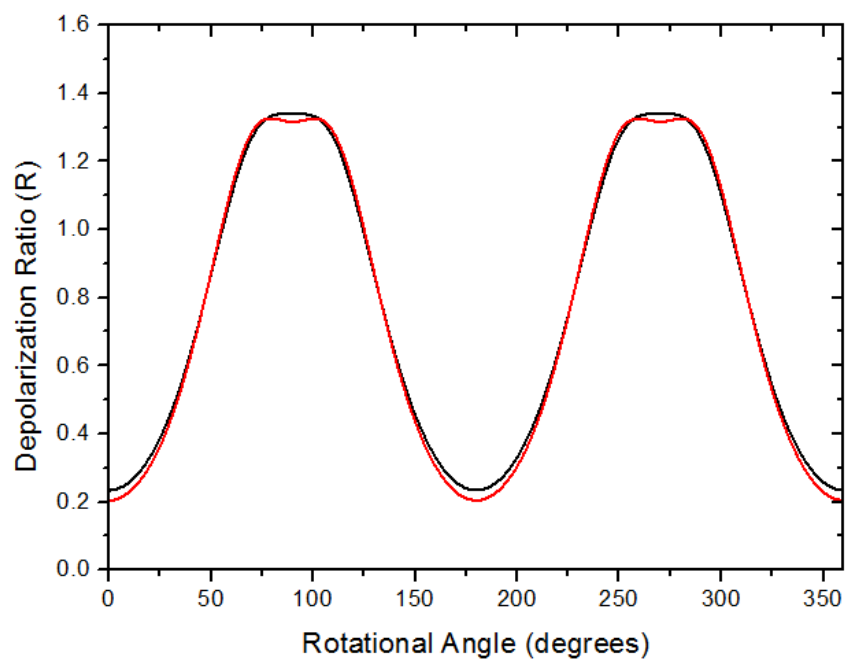
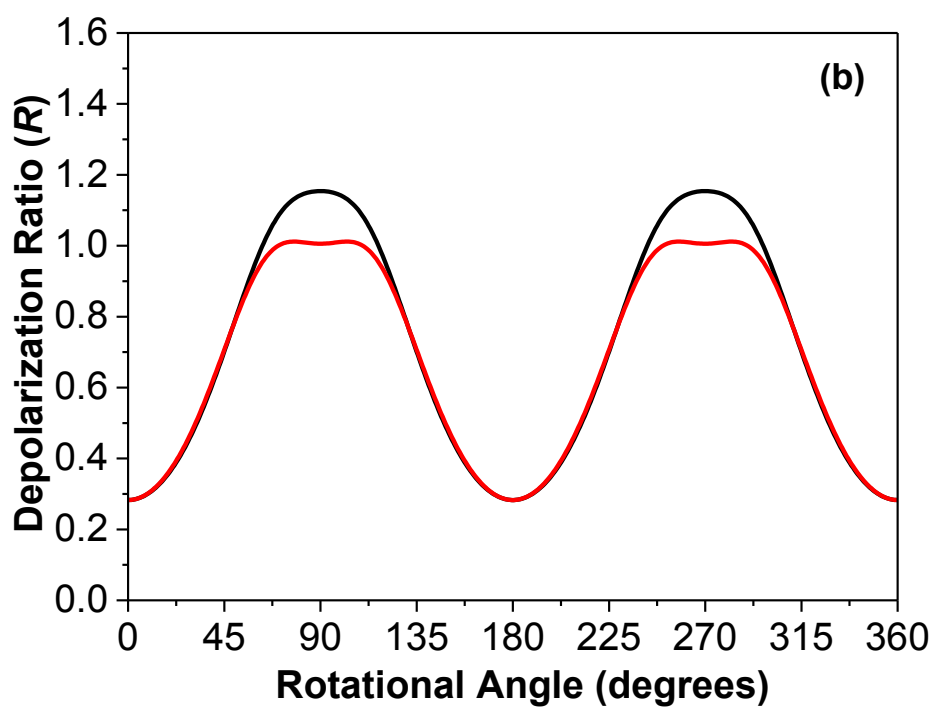
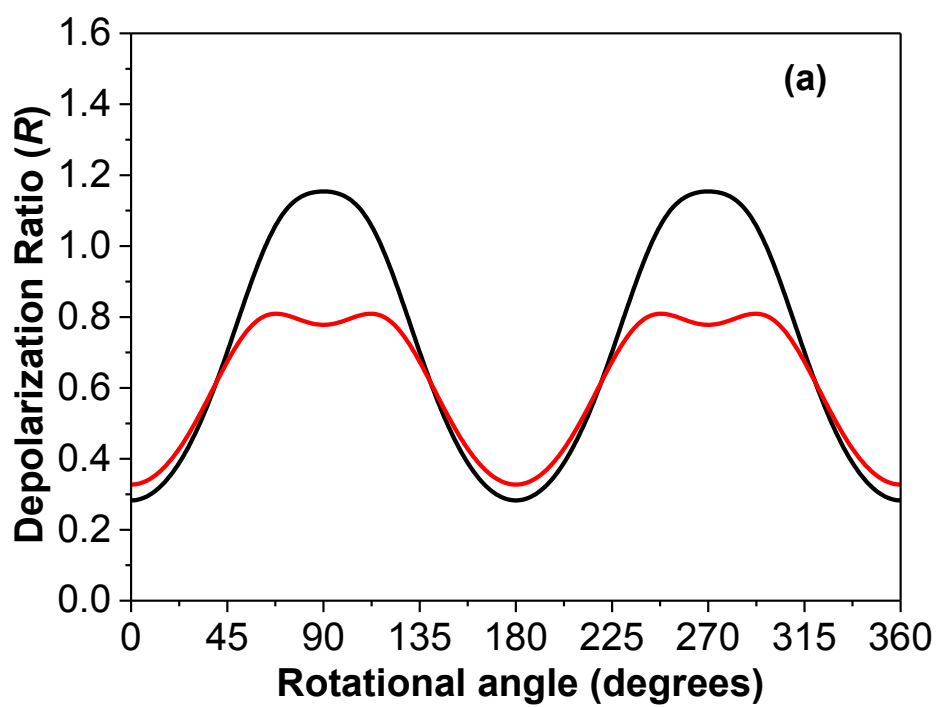


Fig. 9 (Online colour) The depolarisation ratio, R plotted as a function of rotational angle around the optical axis of the laser beam at $T - T_{\text{ISmA}_d} = -21^\circ\text{C}$. The black line comes from the calculation based on the low fitting value of order parameter obtained in Fig. 7 ($\langle P_2 \rangle = 0.496$; $\langle P_4 \rangle = 0.153$; $r = -0.294$ and $\Omega = 120^\circ$). The red line comes from the fitting of the solid black line in Fig. 7 ($\langle P_2 \rangle = 0.535$; $\langle P_4 \rangle = 0.188$; $r = -0.284$ and $\Omega = 118^\circ$).



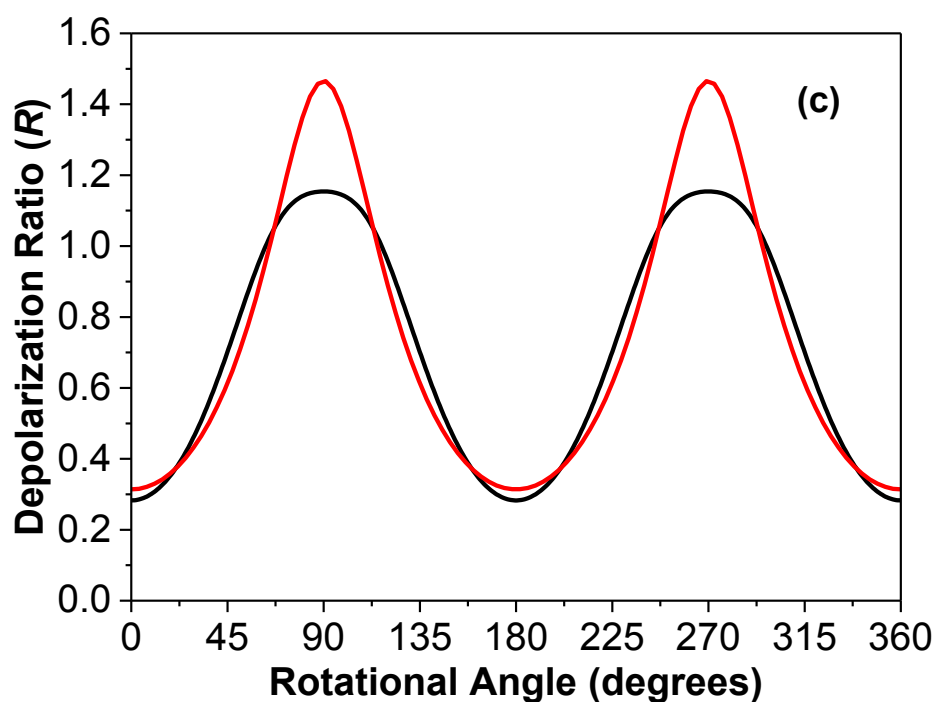


Fig. 10 (Online colour) Illustration of the effect of the biaxial order parameters $\langle P_{220} \rangle$, $\langle P_{420} \rangle$ and $\langle P_{440} \rangle$ on the depolarisation ratio, R . (a) $\langle P_{420} \rangle$ and $\langle P_{440} \rangle$ fixed to be zero and $\langle P_{220} \rangle = 0$ (black line) and 0.05 (red line). (b) $\langle P_{220} \rangle$ and $\langle P_{420} \rangle$ fixed to be zero and $\langle P_{440} \rangle = 0$ (black line) and 0.005 (red line). (c) $\langle P_{220} \rangle$ and $\langle P_{440} \rangle$ fixed to be zero and $\langle P_{420} \rangle = 0$ (black line) and 0.005 (red line). The scale for all parts has been kept same to ease comparison.

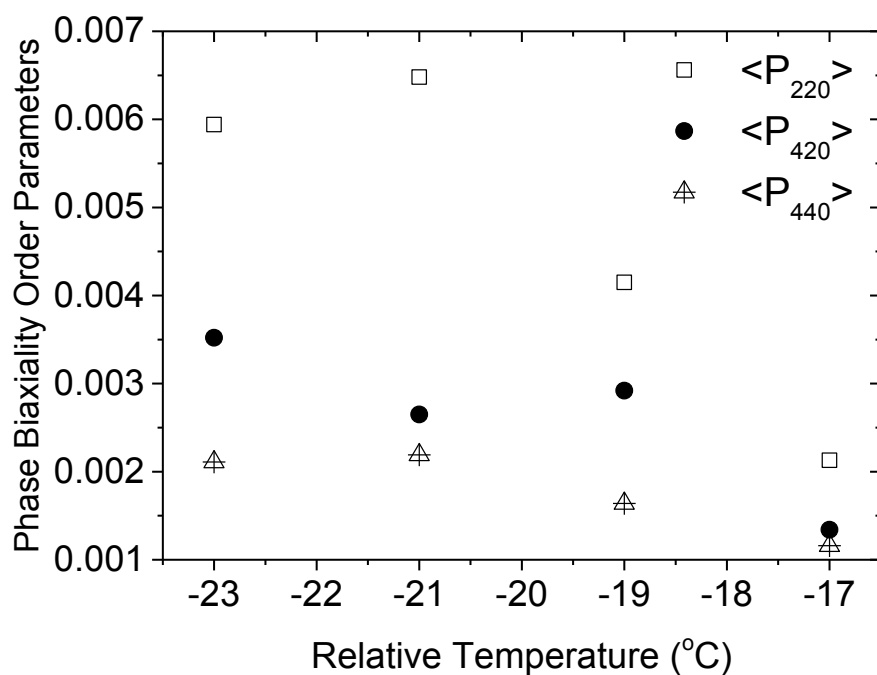


Fig. 11 (Online colour) Fitting values of phase biaxial order parameters as a function of reduced temperature.

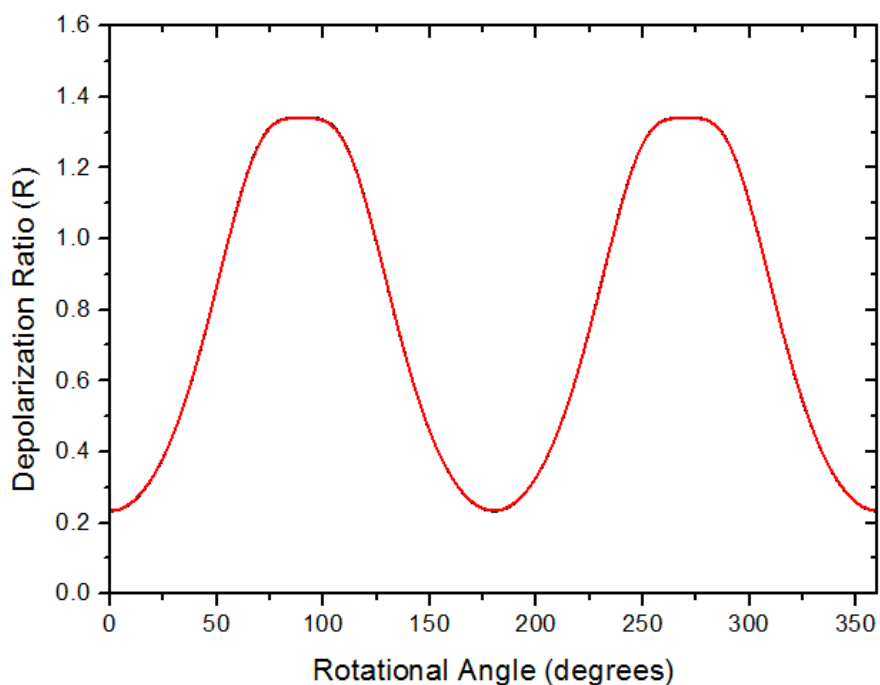
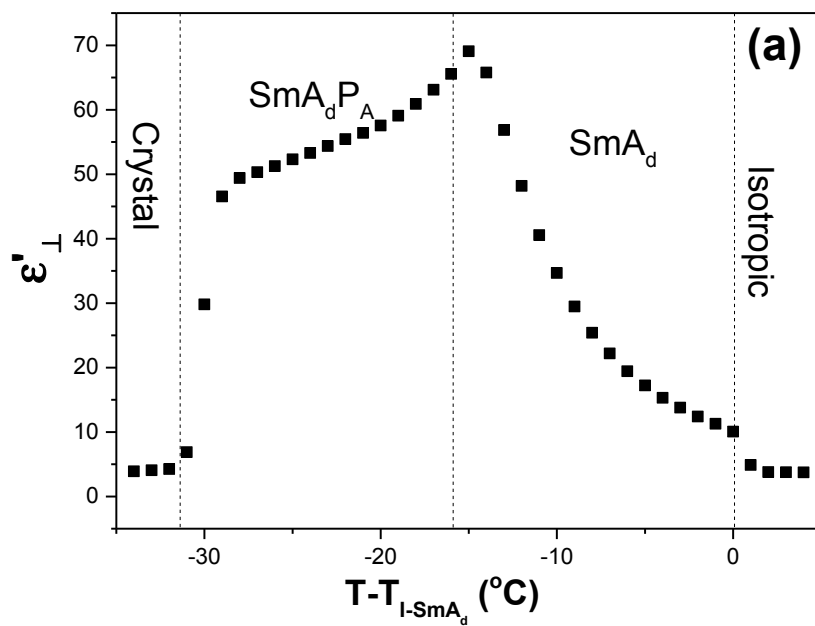
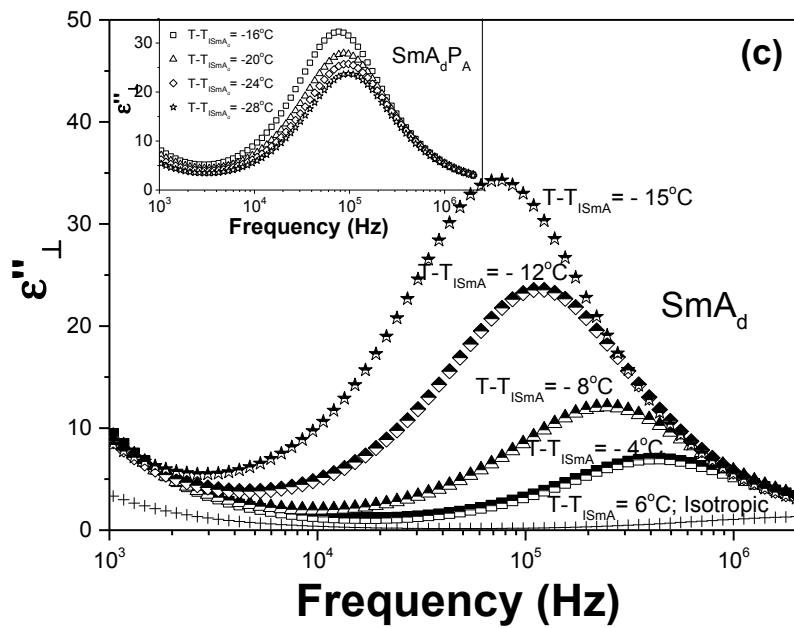
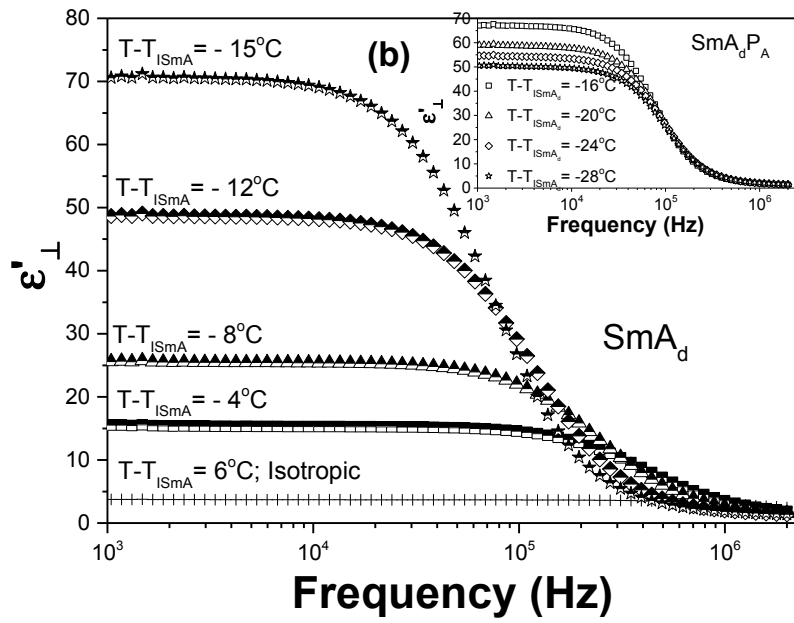


Fig. 12 (Online colour) The depolarisation ratio, R plotted as a function of rotation angle around the axis of the laser beam at $T - T_{\text{ISmA}_d} = -21^\circ\text{C}$. The black line (almost

invisible under the red line) is calculated from the values of order parameter obtained from fitting to the data in Fig.7, i.e., ($\langle P_{200} \rangle = 0.496$; $\langle P_{400} \rangle = 0.153$; $r = -0.294$ and $\Omega = 120^\circ$). The red line is a fit to this in which the uniaxial order parameters are not varied, but are deduced from the estimated curve in Fig. 7. The fitting values that result are ($\langle P_{200} \rangle = 0.535$; $\langle P_{400} \rangle = 0.188$; $\langle P_{220} \rangle = 0.00648$, $\langle P_{420} \rangle = 0.00265$, $\langle P_{440} \rangle = 0.00219$ and $r = -0.299$).





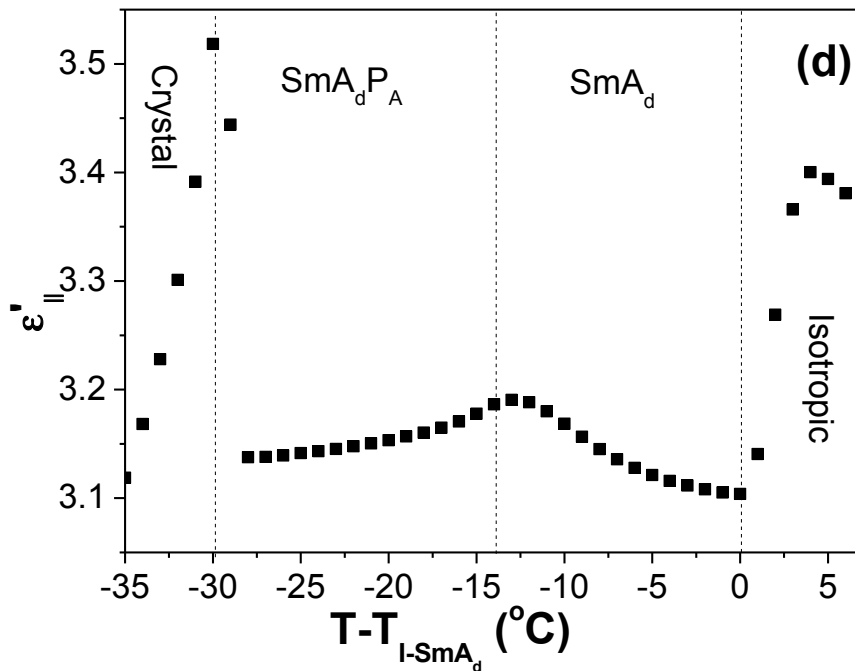


Fig. 13 The real part of perpendicular component of dielectric permittivity ϵ'_{\perp} as a function of (a) temperature at 10 kHz in the various phases (b) frequency at various temperatures in the SmA_d phase (inset shows data in the $SmA_d P_A$ phase), (c) The imaginary part of dielectric permittivity ϵ''_{\perp} as a function of frequency at various temperatures in the SmA_d phase (inset shows data in the $SmA_d P_A$ phase). (d) The real part of the parallel component of dielectric permittivity $\epsilon'_{||}$ as a function of temperature at 10 kHz in the various phases.

1. R. A. Reddy and C. Tschierske, *J. Mater. Chem.*, 2006, **16**, 907.
2. A. Eremin and A. Jákli, *Soft Matter*, 2013, **9**, 615.
3. Y. Matsunaga and S. Miyamoto, *Mol. Cryst. Liq. Cryst.*, 1993, **237**, 311.
4. T. Akutagawa, Y. Matsunaga and K. Yasuhara, *Liq. Cryst.*, 1994, **17**, 659.
5. T. Niori, T. Sekine, J. Watanabe, T. Furukawa and H. Takezoe, *J. Mater. Chem.*, 1996, **6**, 1231.
6. D. R. Link, G. Natale, R. Shao, J. E. Maclennan, N. A. Clark, E. Korblova and D. M. Walba, *Science*, 1997, **278**, 1924.
7. H. Takezoe and Y. Takanishi, *Jpn. J. Appl. Phys.*, 2006, **45**, 597.
8. M. Nagaraj, V. Görtz, J. W. Goodby and H. F. Gleeson, *Appl. Phys. Lett.*, 2014, **104**, 021903.
9. M. Nagaraj, K. Usami, Z. Zhang, V. Görtz, J. W. Goodby and H. F. Gleeson, *Liq. Cryst.*, 2014, **41**, 800.
10. M. Nagaraj, J. C. Jones, V. P. Panov, H. Liu, G. Portale, W. Bras and H. F. Gleeson, *Phys. Rev. E*, 2015, **91**, 042504.
11. G. Dantlgraber, A. Eremin, S. Diele, A. Hauser, H. Kresse, G. Pelzl and C. Tschierske, *Angew. Chem., Int. Ed.*, 2002, **41**, 2408.
12. T. Sekine, T. Niori, M. Sone, J. Watanabe, S. W. Choi, Y. Takanishi and H. Takezoe, *Jpn. J. Appl. Phys.*, 1997, **36**, 6455

13. R. A. Reddy, C. Zhu, R. Shao, E. Korblova, T. Gong, Y. Shen, E. Garcia, M. A. Glaser, J. E. Maclennan, D. M. Walba and N. A. Clark, *Science*, 2011, **332**, 72.
14. A. Eremin, S. Diele, G. Pelzl, H. Nadası, W. Weissflog, J. Salfetnikova and H. Kresse, *Phys. Rev. E*, 2001, **64**, 051707.
15. R. J. Mandle, E. J. Davis, C.-C. A. Voll, D. J. Lewis, S. J. Cowling and J. W. Goodby, *J. Mater. Chem. C*, 2015, **3**, 2380.
16. B. K. Sadashiva, R. Amaranatha Reddy, R. Pratibha and N. V. Madhusudana, *Chem. Commun.*, 2001, 2140.
17. B. K. Sadashiva, R. Amaranatha Reddy, R. Pratibha and N. V. Madhusudana, *J. Mater. Chem.*, 2002, **12**, 943.
18. D. Pocięcha, M. Čepič, E. Gorecka and J. Mieczkowski, *Phys. Rev. Lett.*, 2003, **91**, 185501.
19. M. Gupta, S. Datta, S. Radhika, B. K. Sadashiva and A. Roy, *Soft Matter*, 2011, **7**, 4735.
20. T. Hegmann, J. Kain, S. Diele, G. Pelzl and C. Tschierske, *Angew. Chem. Int. Ed*, 2001, **40**, 887.
21. R. Pratibha, *Science*, 2000, **288**, 2184.
22. K. J. K. Semmler, T. J. Dingemans and E. T. Samulski, *Liq. Cryst.*, 1998, **24**, 799.
23. R. Amaranatha Reddy and B. K. Sadashiva, *J. Mater. Chem.*, 2004, **14**, 310.
24. H. N. Shreenivasa Murthy and B. K. Sadashiva, *Liq. Cryst.*, 2004, **31**, 567.
25. C. Tani, *App. Phys. Lett.*, 1971, **19**, 241.
26. D. Coates, W. A. Crossland, J. H. Morrissy and B. Needham, *J. Phys. D Appl. Phys.*, 1978, **11**, 2025.
27. H.-Y. Chen, R. Shao, E. Korblova, W. Lee, D. M. Walba and N. A. Clark, *Appl. Phys. Lett.*, 2007, **91**, 163506.
28. H.-Y. Chen and J.-S. Wu, *J. Soc. Inf. Disp*, 2010, **18**, 415.
29. S. Jen, N. A. Clark, P. S. Pershan and E. B. Priestley, *Phys. Rev. Lett.*, 1973, **31**, 1552.
30. S. Jen, N. A. Clark, P. S. Pershan and E. B. Priestley, *J. Chem. Phys.*, 1977, **66**, 4635.
31. W. J. Jones, D. K. Thomas, D. W. Thomas and G. Williams, *J. Mol. Struct.*, 2002, **614**, 75.
32. W. J. Jones, D. K. Thomas, D. W. Thomas and G. Williams, *J. Mol. Struct.*, 2004, **708**, 145.
33. C. D. Southern and H. F. Gleeson, *E. Phys. J. E*, 2007, **24**, 119.
34. C. D. Southern, P. D. Brimicombe, S. D. Siemianowski, S. Jaradat, N. Roberts, V. Görtz, J. W. Goodby and H. F. Gleeson, *E. Phys. Lett.*, 2008, **82**, 56001.
35. H. F. Gleeson, C. D. Southern, P. D. Brimicombe, J. W. Goodby and V. Görtz, *Liq. Cryst.*, 2010, **37**, 949.
36. Z. Zhang, V. P. Panov, M. Nagaraj, R. J. Mandle, J. W. Goodby, G. W. Luckhurst, J. C. Jones and H. F. Gleeson, *J. Mater. Chem. C*, 2015, **3**, 10007.
37. H. S. Chang, S. Jaradat, H. F. Gleeson, I. Dierking and M. A. Osipov, *Phys. Rev. E*, 2009, **79**, 0617061-0617069.
38. S. K. Sarkar, P. C. Barman and M. K. Das, *Inter. J. Res. Appl. Nat. Soc. Sc.*, 2013, **1**, 1.
39. B. Kundu, R. Pratibha and N. V. Madhusudana, *Eur. Phys. J. E*, 2010, **31**, 145.
40. S. T. Lagerwall, P. Rudquist and F. Giesselmann, *Mol. Cryst. Liq. Cryst.*, 2009, **510**, 148.
41. H. F. Gleeson and P. D. Brimicombe, *Phys. Rev. Lett.*, 2011, **107**, 109801.

42. F. G. M. Buivydas, G. Andersson, S. T. Lagerwall, B. Stebler, J. Boè Melburg, G. Heppke, B. Gestblom, *Liq. Cryst.*, 1997, **23**, 723.
43. M. Krueger and F. Giesselmann, *Phys. Rev. E*, 2005, **71**, 041704.
44. L. Guo, S. Dhara, B. K. Sadashiva, S. Radhika, R. Pratibha, Y. Shimbo, F. Araoka, K. Ishikawa and H. Takezoe, *Phys. Rev. E*, 2010, **81**, 011703.
45. M A Osipov and G Pajak, *Eur.Phys. J. E*. 2014, **37**: 79